

A longitudinal Bayesian framework for estimating causal dose-response relationships

Yu Luo*, Kuan Liu†, Ramandeep Singh‡, Daniel J. Graham§

Abstract

Existing causal methods for time-varying exposure and time-varying confounding focus on estimating the average causal effect of a time-varying binary treatment on an end-of-study outcome. Methods for estimating the effects of a time-varying continuous exposure at any dose level on the outcome are limited. We introduce a scalable, non-parametric Bayesian framework for estimating longitudinal causal dose-response relationships with repeated measures. We incorporate the generalized propensity score either as a covariate or through inverse-probability weighting, formulating two Bayesian dose-response estimators. The proposed approach embeds a double non-parametric generalized Bayesian bootstrap which enables a flexible Dirichlet process specification within a generalized estimating equations structure, capturing temporal correlation while making minimal assumptions about the functional form of the continuous exposure. We applied our proposed approach to a motivating study of monthly metro-ridership data and COVID-19 case counts from major international cities, identifying causal relationships and the dynamic dose-response patterns between higher ridership and increased case counts.

Keywords: Dose-response relationship; Generalized Bayesian bootstrap; Dirichlet processes; Longitudinal data analysis; COVID-19; Transportation engineering;

*Department of Mathematics, King's College London, U.K.

†Institute of Health Policy, Management and Evaluation, University of Toronto, Canada.

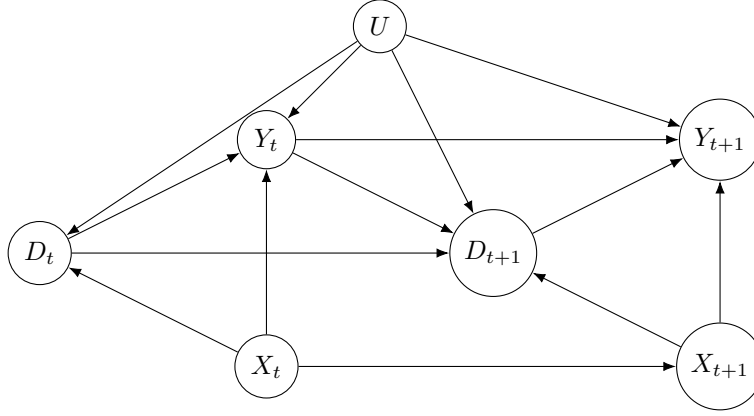
‡Chair of Transportation Systems Engineering, Technical University of Munich, Germany.

§Department of Civil and Environmental Engineering, Imperial College London, U.K.

1 Introduction

The SARS-CoV-2 virus pathogen, which causes the COVID-19 disease, is considered to transmit via two main pathways: (i) directly through droplets and aerosols, and (ii) indirectly through fomite transmission (for example, Derqui et al., 2023). Public transport modes serving dense urban areas induce prolonged exposure for passengers in enclosed and oftentimes poorly ventilated spaces, and they also facilitate the mixing of populations at the origin and destination trip-ends. Consequently, we can reasonably hypothesise that public transport is a vector of virus transmission in a city. While this hypothesis seems intuitively reasonable, and has been put forward previously, including in the mass media (Thomas et al., 2022), it remains largely unsubstantiated statistically under the causal lens. Existing empirical studies quantifying the dynamic impact of mass public transport on COVID-19 transmission are scarce. Most previous studies have analyzed aggregate human mobility, rather than mass transit ridership specifically, for instance, using less granular mobile phone data sources such as those available via Google Mobility or Apple Maps. Despite growing evidence of multi-layered causal pathways, the causal dynamics connecting mass transit ridership, such as metro ridership, to infectious-disease spread remain underexplored.

Figure 1: Longitudinal causal DAG between the mass of metro ridership (treatment variable, D), confounders (X) and the number of COVID-19 cases (Y) from time t to $t + 1$. U represents the source of time-invariant unobserved confounding.



Using the standard causal inference notation, we define our problem in relation to the triple (Y, D, X) , indexed by t to denote time: where Y is the outcome (COVID-19 cases in the city), D is the treatment (urban mass transit ridership), X is a set of time-varying confounders, and U is a set of confounders that are time-invariant. We are interested in the causal effects of D on Y . Figure 1 shows a directed acyclic graph (DAG) of our assumed time-varying causal relationships between mass transit ridership and disease propagation at the city level. The figure shows an autoregressive structure in Y , along with contemporaneous and lagged structure in both treatment effect and confounding. Therefore, we face two key challenges in estimating this causal effect. First, we must adjust for the existence of confounding influences, X and U , which determine both transit ridership and disease propagation. These include time-varying (i.e., X) factors such as the severity of containment measures on human mobility (e.g. lockdown measures), urban mobility characteristics, and vaccination rates, along with a set of

unmeasured time-invariant (i.e., U) city level attributes such as characteristics of the built-environment, urban culture, and baseline socio-demographics. Second, there are dynamic effects presented such that past outcomes act as contemporaneous confounders. Thus, we observe a repeatedly measured outcome, a time-dependent treatment and a set of dynamic time-varying and time-invariant confounders. For estimation, we have monthly (longitudinal) city level data available which measure Covid cases, mass transit ridership, mobility containment measures, and a set of mobility characteristics for the period between 1 March 2020 and 23 January 2022. Longitudinal data provide the temporal resolution needed to understand how public transit ridership and COVID-19 incidence evolve and intersect. To determine causality between the repeatedly measured COVID-19 cases and public transportation ridership, we thus require a robust model that explicitly builds the temporal dependencies illustrated in Figure 1.

Most existing methods for causal estimation of a continuous-exposure are developed for the point-treatment framework, including the generalized propensity score-based (GPS) approaches (Robins et al., 2000; Hirano and Imbens, 2004; Galvao and Wang, 2015), g-computation and outcome regression-based approaches (Hill, 2011), and a doubly robust estimator considering combining both treatment and outcome models (Kennedy et al., 2017). Extensions to longitudinal causal data are very limited and restricted to the parametric frequentist paradigms (Robins et al., 2000; Vansteelandt and Sjolander, 2016). The Bayesian lens for longitudinal causal dose-response analysis is largely missing and remains underexplored in the literature. The Bayesian estimation framework can offer both statistical and practical advantages, such as the propagation of uncertainty through complex model structures and the ability to provide probabilistic summaries of causal effects for intuitive causal decision-making in applied research. In addition, it allows for the incorporation of subjective prior beliefs about the treatment effect and confounding from prior scientific knowledge.

In this paper, we fill this literature gap by presenting a flexible yet computationally tractable generalized double non-parametric Bayesian estimation framework that estimates the entire longitudinal dose-response surface while making minimal distribution assumptions about the functional form of the continuous exposure. Our specific methodological contributions in this paper are on three fronts: i) we introduce the generalized double non-parametric Bayesian estimation framework for dose-response causal analysis with longitudinal data, integrating a similar moment-based restrictions to generalized estimating equations with Bayesian uncertainty propagation; ii) we demonstrate the validity of our approach by showing the theoretical basis behind how the approximate frequentist estimation has a natural Bayesian analogue that rests on equally weak assumptions; and iii) we provide computationally scalable algorithms and open-source code making the proposed Bayesian approach practical for large, real-world datasets for wide adoption and application beyond the motivating study.

The remainder of this paper is organized as follows. In Section 2, we review methods for causal analysis of longitudinal data with repeated outcomes and introduce a nonparametric Bayesian formulation for inference when the model is specified through estimating equations. Section 3 presents simulation studies, where we compare a weighting method and an approach that includes the GPS as a covariate. In Section 4, we apply our methods to an empirical study, analyzing the causal effect of mass transit ridership on the spread of COVID-19. Finally, we conclude with some remarks in Section 5.

2 Methodology

2.1 Causal inference for longitudinal data with repeated outcomes

In the causal inference setting, let $Z_i = (Y_i, D_i, X_i), i = 1, \dots, n$, where for the i th unit of observation Y_i denotes a response, D_i the treatment received which can take values in some bounded interval, \mathcal{D} in \mathbb{R} , and X_i a vector of pre-treatment covariates or confounder variables. Under an experimental design \mathcal{E} , we know that $D_i \perp_{\mathcal{E}} X_i$ with the marginal distribution of D_i , $f_{\mathcal{E}}(d_i)$ known as a constant. However, in observational studies, \mathcal{O} , $D_i \not\perp_{\mathcal{O}} X_i$ and an appropriate adjustment is required to estimate causal effects. Under the potential outcome framework, the observed outcome is, $Y_i = \sum_{d \in \mathcal{D}} \mathbb{1}_{(D_i=d)} Y_i(d)$, where $\mathcal{Y}_i = \{Y_i(d) : d \in \mathcal{D}\}$, is set of all potential outcomes. We assume that the treatment assignment is ignorable, $D_i \perp_{\mathcal{O}} \mathcal{Y}_i | X_i$, and we also assume that the potential outcomes \mathcal{Y}_i are not affected by any other subjects, which is termed the stable unit-treatment value assumption (SUTVA). The primary focus of our inference is average potential outcomes (APOs) for a population under \mathcal{O} , i.e., $\mathbb{E}[Y_i(d)]$, given a specific dose/treatment d . In the longitudinal setting, we wish to study the APO of a longitudinal exposure pattern, over K intervals, on a repeatedly measured outcome. We have for $i = 1, \dots, n$, the observed data can be written as $Z_i = (X_{i1}, D_{i1}, Y_{i1}, X_{i2}, D_{i2}, Y_{i2}, \dots, X_{iK}, D_{iK}, Y_{iK})$, where D_{ik} is the treatment variable for individual i at time k , X_{ik} is the confounder measured prior to the treatment at time k for individual i , and Y_{ik} is the corresponding outcome.

We denote the observed covariate history \bar{x}_k as $\bar{x}_k = (x_1, x_2, \dots, x_k)$. Following Robins et al. (2000), we assume that $Y(d_k) \perp D_k | \bar{X}_k$, which is equivalent to the assumption of no unmeasured confounders in the cross-section analysis. Based on the observable, the joint distribution for individual i is

$$f(z_i | \xi) = \prod_{k=1}^K f_{\mathcal{O}}(y_{ik} | d_{ik}, x_{ik}; \xi) f_{\mathcal{O}}(d_{ik} | x_{ik}; \gamma) f_{\mathcal{O}}(x_{ik}) \quad (1)$$

where $f_{\mathcal{O}}(d_{ik} | x_{ik}; \gamma) \equiv e(x_{ik}; \gamma)$ represents the PS model and $f_{\mathcal{O}}(y_{ik} | d_{ik}, x_{ik}; \xi)$ is the outcome mean model. In line with standard practice in the causal inference, we do not aim to model the marginal distribution $f_{\mathcal{O}}(x_{ik})$. The PS in this case will retain the balancing property, that is, $X_k \perp D_k | e(x_k; \gamma)$. Graham et al. (2014) proposed a longitudinal mixed model extension of the generalized propensity score estimator to handle time-varying confounding and bi-directionality between treatment and outcome. The two-step approach first uses a random intercept in the marginal PS model to adjust for time-invariant confounding, followed by an outcome regression model incorporating the estimated PS. This procedure yields consistent estimates of the APO if the PS models are correctly specified. Building on this approach, we can model the marginal outcome distribution by incorporating the estimated PS. The marginal structural model uses subject-visit-specific weights to create a pseudo-population in which treatment is independent of covariates and outcome history (Liu et al., 2020). The marginal treatment effect can then be estimated using a generalized estimating equation (GEE), defined by the following estimating equation

$$\sum_{i=1}^n \mathbf{U}_i(\xi) = \sum_{i=1}^n \left(\frac{\partial u(x_i, d_i, e(x_i, \hat{\gamma}), \xi)}{\partial \xi} \right)^{\top} \Sigma_i^{-1} (y_i - u(x_i, d_i, e(x_i, \hat{\gamma}), \xi)) = 0 \quad (2)$$

where y_i is a vector of observed response for i th subject. The function $u_i(x_i, d_i, e(x_i, \hat{\gamma}), \xi)$ is the marginal conditional mean model of y_i with the estimate PS via a longitudinal model, such as a mixed effect model (Graham et al., 2014) or a GEE (Liu et al., 2020). This connects the targeting parameter ξ from a link function, and Σ_i is the $(K + 1) \times (K + 1)$ working covariance matrix for subject i . However, as noted in Tchetgen et al. (2012), the GEE approach consistently estimates the parameters of a correctly specified regression model in absence of weights, irrespective of whether the working correlation structure is correct. The GEE framework offers flexibility in targeting the marginal treatment effect for repeated measurements. However, its reliance on estimating equations, rather than full likelihoods, poses challenges for conventional Bayesian analysis, as there is no explicit distributional form for the marginal mean model. This motivates the development of a fully Bayesian approach, which we outline in the next section.

2.2 Bayesian non-parametric method

The Bayesian framework offers calibrated uncertainty quantification and prediction, which can render a more thorough understanding of the causal effect from a practical perspective. There is growing interest in the application of Bayesian methodology to causal problems, but most proposed methods appeal to the principles of PS-adjustment or flexible outcome modeling (Stephens et al., 2023; Li et al., 2023). An advantage of the Bayesian approach for estimation of these models is that estimated causal effects are in the form of distributions, rather than point estimates, allowing us to make probability statements about the causal quantities of interest (i.e., APOs). For example, we can specify parametric outcome model and PS model in (1) and then draw inference based on the posterior sample. This is challenging in the causal setting as the GEE model (2) is only partially specified via the conditional mean without specification of the distribution model. We have to examine procedures for Bayesian inference in the case where we wish to perform analysis of an approximate model, acknowledged to be misspecified compared to the data generating model. Suppose we assume that there is a set of estimating equations $\mathbf{U}(\xi)$ of functions such that $\mathbb{E}[\mathbf{U}(\xi) | \xi] = 0$, for all ξ . The objective is to find a non-parametric approximate model, $p(z)$, to the true data generating model $f(z|\xi)$. Thus, we can define some discrepancy $\delta(f|p)$, subject to $\int \mathbf{U}(\xi) p(z) dz = 0$ and $\int p(z) dz = 1$. The problem then becomes

$$\min_p \delta(f|p) \text{ subject to } \int \mathbf{U}(\xi) p(z) dz = 0, \int p(z) dz = 1, \forall \xi \in \Xi. \quad (3)$$

Suppose $p(z)$ is discrete as nonparametric probabilities as p_i . Then we can deduce the problem as the following constrained optimization problem

$$\min_{p_1, \dots, p_n} \delta(f|p_1, \dots, p_n) \text{ subject to } \sum_{i=1}^n p_i = 1, p_i \geq 0, \sum_{i=1}^n p_i \mathbf{U}_i(\xi) = \mathbf{0}. \quad (4)$$

From a non-parametric viewpoint, we need to consider placing the prior distribution for this non-parametric approximate model, p . In the next section, we link this prior specification to the Bayesian bootstrap framework and a generalized version, which enables us to derive the posterior distribution of ξ by solving the constraint in (3) in a functional form.

2.3 The generalized Bayesian bootstrap

If we consider models without the moment constraint in (4), then the solution will be the empirical distribution, i.e., $p_i = 1/n$. Solving the moment constraint with $p_i = 1/n$ yields a point estimate for ξ . If we place a prior on p_i and allow p_i to vary, it implicitly gives a functional form of $\xi(F)$. This is reminiscent of the classical formulation of the Bayesian bootstrap, which assumes that the data points are realizations from a multinomial model on the finite set $\{z_1, \dots, z_n\}$ with unknown probability $\mathbf{p} = (p_1, \dots, p_n)$, and assuming a priori that $\mathbf{p} \sim \text{Dirichlet}(\alpha, \dots, \alpha)$, then, a posteriori $\mathbf{p} \sim \text{Dirichlet}(\alpha + 1, \dots, \alpha + 1)$. The standard Bayesian bootstrap is obtained under the improper specification $\alpha = 0$ (Rubin, 1981). Therefore, if we repeatedly sample $\mathbf{p} \sim \text{Dirichlet}(1, \dots, 1)$, then

$$\begin{aligned} \sum_{j=1}^n p_j \mathbf{U}_1(x_j, d_j, \gamma) &= \mathbf{0} \\ \sum_{j=1}^n p_j \mathbf{U}_2(z_j, \xi, e(x_j, \hat{\gamma})) &= \mathbf{0}, \end{aligned} \tag{5}$$

where the GEE, $\mathbf{U}_1(\cdot)$, is the estimating equation related to the propensity score model, and $\mathbf{U}_2(\cdot)$ is the GEE for the OR model, and $\hat{\gamma}$ is the solution to (5). Therefore, we can obtain the posterior distribution of ξ under this limiting specification (Newton and Raftery, 1994; Chamberlain and Imbens, 2003).

Motivated by this limiting case, we extend the Bayesian bootstrap to a more general Dirichlet process (DP) specification. If the approximating model, p , is parameterized by the true but unknown distribution, we can specify a priori $P \sim DP(\alpha, G_0)$ where $\alpha > 0$ is the concentration parameter and G_0 is the base measure. In light of data (z_1, \dots, z_n) , the resulting posterior distribution of P is $DP(\alpha_n, G_n)$, where $\alpha_n = \alpha + n$ and $G_n(\cdot) = \alpha G_0(\cdot) / (\alpha + n) + \sum_{j=1}^n \delta_{z_j}(\cdot) / (\alpha + n)$. Specifically, we can generate the collection of data from the DP via $\{z_j\}_{j=1}^\infty \sim G_n$ and $\{p_k\}_{k=1}^\infty \sim \text{StickBreaking}(\alpha_n)$; the standard stickbreaking algorithm (Sethuraman, 1994) generates the weights by a transformation of the collection $\{V_k\}_{k=1}^\infty$ where $V_j \sim \text{Beta}(1, \alpha)$ are independent, with $p_1 = V_1$ and for $j = 2, 3, \dots$, $p_j = V_j \prod_{k=1}^{j-1} (1 - V_k)$. Therefore, to obtain a posterior variate, we can sample $\{z_j^s\}_{j=1}^\infty \sim G_n$ and $\{p_j\}_{j=1}^\infty \sim \text{StickBreaking}(\alpha_n)$, then solving

$$\sum_{j=1}^\infty p_j \mathbf{U}_1(x_j^s, d_j^s, \gamma) = \mathbf{0}, \sum_{j=1}^\infty p_j \mathbf{U}_2(z_j^s, \xi, e(x_j, \hat{\gamma})) = \mathbf{0}. \tag{6}$$

Although this is an infinite sum, the p_j decreases in expectation as j increases and eventually becomes numerically negligible. Because of this decay, the infinite sum can be truncated at some finite J , such that $p_J < \epsilon$ for a small tolerance ϵ . The uncertainty about ξ is properly addressed in this ‘forward’ calculation. We also layout this DP specification for the longitudinal analysis in Algorithm 1. In this formulation, we do not directly specify a prior for ξ but instead it is a functional of p_i , where we carry out a fully Bayesian inference for p_i . This approach is computationally more efficient because it relies purely on optimization instead of MCMC, which provides a ‘shortcut’ to fully Bayesian causal inference. The validity and theoretical justification of this approach have been thoroughly examined in cross-sectional settings in Luo et al. (2023).

Data: $z_{1:n} = (z_1, \dots, z_n)$

Given α and G_0 , **for** s **to** $1 : S$ **do**

- Sample a new collection of data $\{z_k^s\}$ with probability $1/(\alpha + n)$ from z_i and probability $\alpha/(\alpha + n)$ from G_0 ;
- Sample $\{p_k^s\}$ from a stick-breaking process with $\alpha_n = \alpha + n$;
- Estimate the PS based the GEE related to \mathbf{U}_1 in (6) with the data $\{z_k^s\}$ and the weight $\{p_k^s\}$;
- Solve the GEE related to \mathbf{U}_2 in (6) and obtain ξ^s with the data $\{z_k^s\}$, the weight $\{p_k^s\}$ and the estimated PS;
- Compute the APO, $\zeta^s(d)$, at a given dose level d based on the sample ξ^s and the estimated PS.

end

return $(\zeta^1(d), \dots, \zeta^S(d))$.

Algorithm 1: Algorithm for generating posterior samples of the APO at a given dose level d based on the generalized Bayesian bootstrap (DP specification).

3 Simulations

In this section, we examine the performance of the methods described in Section 2 in different aspects. We consider the following models for our simulation studies.

- WOR-BB: The weighted estimating function approach using the GPS as the weight combined with the Bayesian bootstrap framework.
- COV-BB: The estimation function generated by including GPS in the outcome model combined with the Bayesian bootstrap framework.
- WOR-DP: The weighted estimating function approach using the generalized propensity score as the weight combined with the DP framework ($\alpha = 5$).
- COV-DP: The estimation function generated by including propensity scores in the outcome model combined with the DP framework ($\alpha = 5$).

3.1 Example 1

In this example, we conduct a simulation study on a sample size of 100 individuals, each with 10 time points and a total of 1000 observations. We generate the data via the following relationships:

$$X_{1it} \sim \mathcal{N}(0.2, 0.1), X_{2it} \sim \mathcal{N}(1, 0.6), U_i \sim \mathcal{N}(0.2, 0.1), D_{it}|X_{1it}, X_{2it}, U_i \sim \mathcal{N}(1 + 4X_{1it} + 2X_{2it} + U_i, 1)$$

$$Y_{it}|D_{it}, X_{1it}, X_{2it}, U_i \sim \mathcal{N}(20 \exp[D_{it} + X_{1it} - 0.25X_{2it} + 0.5U_i], 1)$$

D is a continuous treatment variable, and X_1, X_2 are time-varying confounders and U is a time-invariant confounder for D with a nonlinear relationship in Y . The goal of this causal setting is to estimate the APO, i.e., the outcome at a specific dose level. We consider estimating the dose-response relationship based on a GEE model for GPS with the inclusion of covariates X_{1it}, X_{2it} only. For the COV method, we fit a GEE model for the outcome of $\log Y_i$ with the inclusion of covariates D_{it} , the three-order spline of estimated GPS. As for WOR method, we fit the outcome mean with the three-order spline of D_{1it} with the GPS as the weight. In the DP method, the new data are generated from the old dataset or new data (unseen) from the base measure, G_0 . We generate these new data through residuals arising from the outcome model. In this case, we first draw each pair of $\{y_{ik}^{s'}, (x_{ik}^s, d_{ik}^s)\}$, $k = 1, \dots, K_i, i = 1 \dots, N$, from the empirical distribution as the DP with $\alpha = 0$, and then obtain the GPS, $e(x_{ik}^s; \hat{\gamma}^s)$ from a mixed effect model with the inclusion of covariates x_{1it}^s, x_{2it}^s to account for the effect of the unmeasured confounder (Graham et al., 2014), refitted to the newly sampled $\{(x_i^s, d_i^s)\}$ data set. Then we simulate $y_i^s = \{y_{ik}^s\}_{k=1}^K$ from a DP model with the conditional base measure $G_0 \equiv \mathcal{N}_K(\mu(x_i^s, e(x_i^s; \hat{\gamma}^s)), 1)$, where $\mu(x_i^s, e(x_i^s; \hat{\gamma}^s))$ is the fitted value from a GEE model with $\log y_i^{s'}$ with the inclusion of covariates d_i^s , the three-order spline of estimated GPS, $e(x_i^s; \hat{\gamma}^s)$. In the stick breaking construction, we truncate the sample size at $J = 500$. The weight is less than 10^{-4} after 500 iterations and can be deemed as negligible.

We first simulate one dataset and generate 1000 posterior samples. Figure 2 shows the 1000 posterior dose-response curves with observed data points. The weighting method results in a larger variance because treatment density measurement can lead to extreme density weights and hence higher variability in the results. This issue becomes particularly obvious in the WOR approach when there are few observations in the tail range, as limited data can result in unstable weight estimates and inflated variance. In comparison, the COV approach is more stable, maintaining a comparatively lower degree of variation by exercising efficient control over the impact of fewer observations. This suggests that COV provides a more reliable estimation framework, especially in scenarios with limited sample sizes. We do not observe any noticeable difference between the BB and DP methods. Subsequently, we repeat this simulation on 1000 datasets, each consisting of 1000 entries, and evaluate the performance on three given doses. The results are shown in Table 1, with averages of the posterior means (Av Est), variances (Av Est Var) and coverage rates based on with the 2.5% and 97.5% posterior sample quantiles. The APO estimates are calculated for doses 3, 4, and 5. The APO estimates in all models are represented via a logarithmic transformation, and the results are also presented in the logarithmic scale. All Bayesian dose-response estimators have approximately unbiased estimates and desired coverage rates, despite these models involving approximations to the true nonlinear dose-response function only including the GPS and the treatment variable. When comparing the variance between the COV and WOR approaches, the WOR method exhibits greater average variability. The DP approach shows slightly lower variance in the WOR method compared to BB, and this is due to its use of a larger resampled dataset, leading to a better representation of sparsely observation regions in the original data. The BB-WOR method yields coverage around 80% which is not optimal, whereas the DP-based approach achieves coverage much closer to the nominal level. Therefore, in this case, the DP approach is preferable for the weighting-based estimator. In summary, this example suggests that the proposed double generalized Bayesian bootstrap method is suitable for handling longitudinal data with repeated measures,

yielding desirable and valid uncertainty quantification.

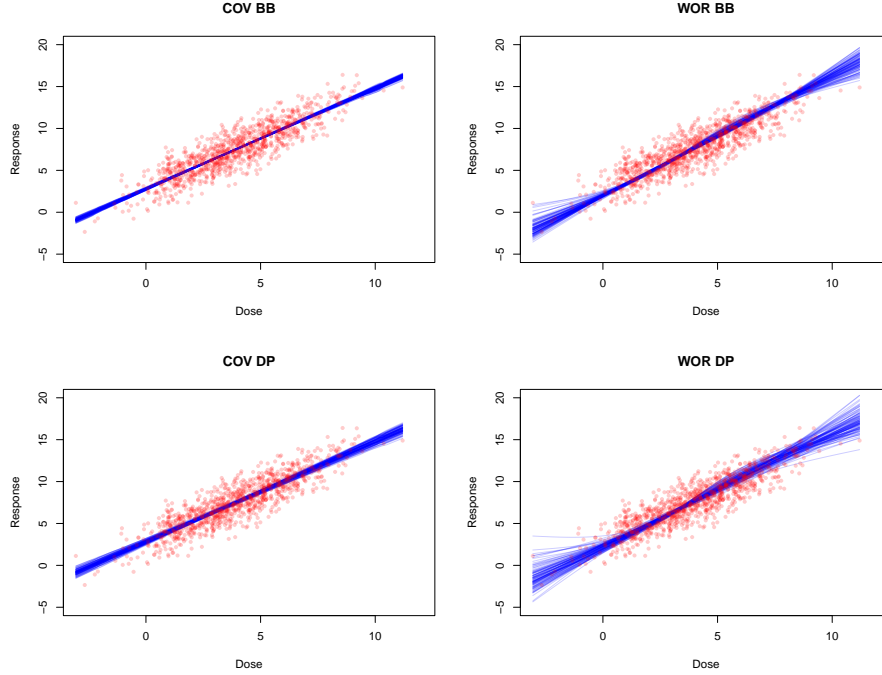


Figure 2: Example 1: Posterior dose-response curves using WOR and COV approaches. The blue curve represents the estimated dose-response curve for one replicate. The red dots represent the observed data.

3.2 Example 2

In this example, we demonstrate inference for simulated outcome as the count data, similar to our real data. All the variables simulated from the same distribution as in Example 1, except the outcome which is generated from a Poisson distribution:

$$Y_{it}|D_{it}, X_{1it}, X_{2i}, U_i \sim \text{Poisson} \left(\exp \left[1 + 0.2D_{it} + 0.005 \frac{X_{1it}}{100} - 0.002 \frac{X_{2it}}{100} + 0.1U_i \right] \right).$$

Similar to the first example, we fit a Poisson GEE model for the outcome of Y_i with the inclusion of covariates D_{1it} , the three-order spline of estimated GPS for COV method, and as for WOR method, we fit the outcome mean with the three-order spline of D_{1it} with the GPS as the weight. For the DP approach, we use the same steps to sample the data with size 500, but the outcome y_i^s then is sample from a Poisson distribution with mean $\mu(x_i^s, e(x_i^s; \hat{\gamma}^s))$, which is the fitted value from a GEE model with $y_i^{s'}$ with the inclusion of covariates d_i^s , the three-order spline of estimated GPS.

Figure 3 demonstrates the 1000 posterior dose-response curves with observed data points. We observe a consistent pattern where the weighting method leads to greater variance, particularly in regions with fewer observations. Similar to the previous example, there is not much difference between the BB and DP approaches. Table 1 summarizes the results of 1,000 simulation runs at three specified dose levels. The COV and WOR methods

both give roughly unbiased estimates for all dose levels. The WOR approach consistently exhibits higher average estimated variances compared to the COV method. When applying the weighting approach, the DP method continues to demonstrate slightly lower variability relative to the BB method. This is likely because the DP resampling scheme yields larger sample sizes, which help stabilize estimates, particularly in regions with sparse data. In terms of coverage performance, the BB-COV procedure performs well at dose level 4, where data are more abundant. However, at other dose levels, where observations are sparse, the coverage rate for the COV method drops substantially. This suggests that the resulting credible intervals may be too narrow in regions with limited data support, leading to undercoverage. On the other hand, the WOR-BB procedure maintains a relatively stable undercoverage rate, ranging from approximately 82 to 85 across all dose levels. However, the DP method consistently achieves coverage around the nominal target across all three dose levels, regardless of whether it is used with the COV or WOR estimating procedure. This result demonstrates that the DP approach better accommodates data sparsity and improves posterior coverage across the dose-response curve.

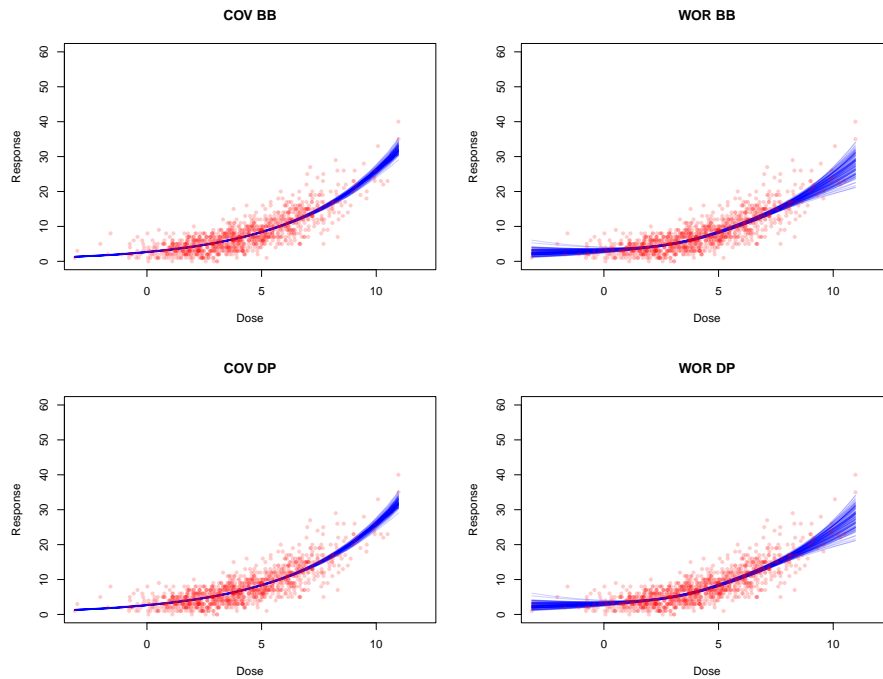


Figure 3: Example 2: Posterior dose-response curves using WOR and COV approaches for the Poisson outcome.

4 Application: Quantifying the causal impact of mass transit on COVID-19 transmission

As discussed in the introduction, empirical studies quantifying the causal impact of mass public transport on COVID-19 transmission are scarce. Most use aggregate measures of mobility from mobile phone data sources such as those that were made publicly available by Google Mobility and Apple Maps during the pandemic, and

issues of causality have received little attention. In our review, we have identified just one empirical study by Romero García et al. (2023) which uses causal analysis methods to assess the impact of travel specifically on metro networks (referred to as subways in the paper) on the transmission of COVID-19 in Valencia, Spain. In the following sections, we provide a summary of empirical studies undertaken on the impact of mobility on COVID-19 transmission, beginning with an overview of literature using non-causal analysis methods, followed by a summary of the limited literature adopting causal methods.

4.1 Non-causal empirical studies

There is a vast number of empirical studies that use non-causal statistical analysis methods to study the association of mobility with COVID-19 transmission as measured by either the number of COVID-19 cases or the virus reproduction number. Generally, most studies conclude that an increase in mobility is positively associated with an increase in COVID-19 transmission, and restrictions on mobility are associated with reductions in COVID-19 transmission. Studies using statistical correlation methods are prevalent in the literature. For example, Jia et al. (2020) reported a positive linear correlation between mobility and case incidence in China at the early stages of the pandemic. Badr et al. (2020) analysed mobility patterns in the USA and also reported positive linear correlations between mobility and COVID-19 case rates. Kissler et al. (2020) used Pearson’s linear correlation coefficient and reported that their estimates of COVID-19 prevalence was negatively associated with reductions in mobility in their analysis of New York City.

Studies adopting different forms of multivariate regression methods are also prevalent, and here we present a selection of examples. Li et al. (2021) used multivariate linear regression and reported that the reproduction number of the virus increased with higher levels of mobility at retail and recreation places, workplaces, and transit stations in the UK. Kraemer et al. (2020) applied a generalized linear regression model framework and found that mobility was positively correlated with case incidence in China prior to travel restrictions, but the relationship was no longer statistically significant after the implementation of restrictions. McGrail et al. (2020) undertook a cross-country analysis of 134 countries and 50 US states. The authors used a generalized linear mixed effects model and reported that mobility and infection rates reduced after the imposition of social distancing restrictions. Islam et al. (2020) also performed a cross-country analysis of 149 countries using a two-stage linear regression analysis. It was reported that case incidence reduced with the imposition of public transport closures, school closures, work closures, restrictions on mass gatherings, and blanket lockdowns. Xiong et al. (2020) reported a positive relationship between mobility and COVID-19 cases in the US using structural equation modelling with dynamic panel and time-varying effects at the level of US counties. Manzira et al. (2022) used a multivariate time series regression model with autoregressive lag effects and reported a positive association between mobility and the incidence of COVID-19 in the city centre areas of Dublin, Ireland.

4.2 Causal empirical studies

There are a limited number of studies that adopt causal analysis methods to quantify the impact of mobility on COVID-19 case transmission. Romero García et al. (2023) undertook the only known analysis of the impact of metro travel on COVID-19 case rates. Romero García et al. (2023) performed a small-scale analysis of the impact of the locations of subway stations and hospitals on COVID-19 cases in Valencia Spain. They first partitioned the region using Voroni diagrams using subway locations and hospitals as segmentation variables, and then applied the Granger causality test. A positive association was reported between interchange subway stations and COVID-19 cases, while transmission from hospital locations generated more mixed results.

Steiger et al. (2021), Nugent and Balzer (2023), Cho et al. (2022), and Chernozhukov et al. (2021) used aggregate indicators of mobility from mobile phone data records unattributed to specific travel modes to assess causality between mobility and COVID-19 cases. Steiger et al. (2021) estimated the causal impact of factors affecting the number of new cases of COVID-19 in Germany using a DAG and a negative binomial regression model. The authors found a positive causal impact between mobility in retail and recreational spaces and workplaces and COVID-19 cases, and a negative causal impact for essential shopping and mobility within residential areas. Other influential factors included weather, socio-demographic characteristics, and public awareness of COVID-19. Nugent and Balzer (2023) adopted the causal modified treatment policy method with the Super Learner machine learning algorithm to quantify the impact of mobility on COVID-19 cases in US counties. The authors found that unadjusted estimates suggested that decreasing mobility is causally linked to decreasing COVID-19 cases, but found that their adjusted estimates gave mixed results indicating potential confounding in the unadjusted estimates, which were most likely attributed to unknown differences in county characteristics. Cho et al. (2022) also analysed the causal relationship between COVID-19 cases and mobility in the US. They adopted an ensemble empirical mode decomposition method with causal decomposition and reported that mobility levels have a causal relationship with long-term variations in COVID-19 cases rather short-term variations. Chernozhukov et al. (2021) used a casual structural model framework to test a range of counterfactual experiments including mobility changes and their impact on COVID-19 cases in the US. The authors find that reductions in mobility due to stay at home orders and business closures were effective in reducing case numbers, while the impacts of reductions in mobility due to school closures were inconclusive.

4.3 Data

The Community of Metros (COMET) benchmarking group administered by the Transport Strategy Centre at Imperial College London have provided ridership data from 8 international member metro networks. In keeping with commercial confidentiality requirements, the metro identities have been anonymized and are referred to with a numerical index ranging from 1 to 8 throughout this paper. The ridership data report the numerical ridership figures for each day. The data are recorded from before the onset of the COVID-19 pandemic to early 2022, with the earliest and latest dates in the data set being 1 March 2020 and 23 January 2022.

Data on COVID-19 case numbers correspond to the city that each metro is located in and refer to daily case numbers. The data on case numbers have been obtained from the Oxford University COVID-19 Government Response Tracker (OxCGRT) (Hale et al., 2021). Additional data from the OxCGRT database included in the analysis are the number of COVID-19 deaths per day, and a metric termed the Stringency Index which represents the severity of policy control measures implemented by governments during COVID-19 to limit transmission. The Stringency Index is a numeric index ranging from 0-100 with higher values corresponding to stricter control measures. We also include data on vaccinations which represent the cumulative total of vaccinations delivered on a daily basis from the our World in Data database (Mathieu et al., 2021). Lastly, we include a series of variables representing all forms of mobility from Google Mobility (Google LLC, 2022), specifically: residential, workplace, retail and recreation, grocery and pharmacy, and parks.

For context, a summary of all variables including their descriptive statistics aggregated across all metros in the analysis is given in Table 2. The ridership is transformed in a logarithmic scale, cases and deaths variables are transformed with $\log(x + 1)$ scale. From our preliminary analysis, the distribution of ridership is highly skewed and therefore we take the right log scale. After the transformation, the distribution looks more normal, and the ridership in log scale will be the treatment variable. For the outcome variable, we will consider to use cases without transformation and in $\log(x + 1)$ scale.

4.4 Results

To estimate the dose-response relationship between the ridership and COVID-19 cases, we employed the proposed Bayesian method to analyze two different outcomes: the raw case counts, modeled using a log link with the Poisson mean-variance relationship, and the log-transformed case counts, $\log(x + 1)$, modeled under an identity with the Gaussian mean-variance relationship. For both outcomes, we specified an independent working correlation structure and included all relevant confounders along with a cubic spline function of the GPS as covariates. Similar to the simulation, for the GPS model, we used a GEE model that adjusts for all time-varying confounders. We generated a total of 5,000 posterior samples. For the DP method, we generate a synthetic dataset of size $J = 200$ using a procedure similar to that employed in the simulation studies. Due to the relatively small sample size, the stick-breaking weights in the DP decreased rapidly, falling below 10^{-8} after approximately 200 iterations. Figure 4 shows the posterior predictive dose-response curves for WOR and COV methods. When using the COV method, we observe an increasing dose-response trend for both outcomes, suggesting that higher metro ridership is associated with a greater rise in COVID-19 cases. However, the variability in the estimates is higher in certain dose ranges (e.g, 10-12 and 14-15). The DP approach shows more stable curve as the synthetic dataset have a larger sample. When using case counts as the outcome, the COV method shows a generally exponential increase in cases as the logarithm of ridership rises. In contrast, the DP method appears to overcompensate in certain regions, resulting in some non-smooth curves likely because some portion of the resampled data is drawn from areas that deviate from the main trend. The WOR method, on the other hand, shows an initial rise in case counts that eventually plateaus and then slightly declines. In regions with sparse data, the DP approach produces more

stable estimates, suggesting improved performance in low-density areas. We also report the estimated APOs at various doses of the posterior sample in Table 3. We choose the dose level at 11, 13 and 15, which corresponds to 2.5%, 50% and 97.5% quantiles of the logarithm of ridership respectively. Similar to the observation in Figure 4, the COV method reveals that the number of cases increases as the logarithm of ridership rises. On average, the number of cases increases from about 7330 to 59000 when dose level changes from 11 to 15, using $\log(\text{case} + 1)$ as the outcome. When modeling the outcome as the count data, the number of cases increases by an even higher extent, from approximately 500000 to 5000000. This increase is attributed to the fact that exponential change when modeling the count data. However, the WOR method shows a different trend. While the number of cases initially increases, it begins to decline as the dose level rises from 13 to 15. In summary, the number of cases tends to increase as the dose level—representing public transport usage—rises, but this relationship seems not strictly linear. While both the log-transformed and count-based outcome suggest a strong upward trend in case numbers at lower dose regions, the log-transformed model shows a more moderate increase due to its smoothing effect, whereas the count model captures a steeper, exponential rise.

5 Discussion

In this paper, we introduced a non-parametric Bayesian framework for estimating longitudinal causal dose-response relationships in the presence of repeated measures. We address the issue of Bayesian inference in the context of model misspecification, and tackle this problem with a constraint optimization where the approximated model needs to satisfy some moment conditions while minimizing some distance between the true data generating model. From this route, we argue that the general Bayesian bootstrap approach with the DP specification is the consequence of the prior on the non-parametric probabilities. Our approach extends traditional Bayesian methodology by incorporating the double non-parametric generalized Bayesian bootstrap, while explicitly capturing the temporal structure of the data through the GEE framework. We model both GPS and the outcome mean via the GEE, and incorporate the GPS into the outcome model in two ways, as a covariate and through weighting. From the simulation studies, both of the resulting Bayesian dose-response estimators exhibit approximately unbiased estimation and achieve nominal posterior coverage rates under a range of scenarios using the DP method. However, the weighting-based estimator tends to have a larger posterior variance and displays greater instability when few observations are available at specific levels of the exposure. This finding corresponds to other similar inverse treatment weighting approaches with continuous exposure where binning of the continuous exposure maybe considered (Naimi et al., 2014). In our empirical study, we investigated the impact of metro ridership on COVID-19 case counts across major urban centers during the pandemic. The results suggest that increased metro ridership contributes to the spread of COVID-19 up to a certain exposure threshold, beyond which the effect plateaus. These findings have important implications for pandemic-related urban policy, particularly in informing lockdown strategies and optimizing transportation systems in future public health crises.

One appealing aspect of Bayesian estimators is their flexibility, as they allow for flexible approaches with minimal

assumptions about the dose-response relationship, and for the prior knowledge to be added in the model. The proposed method can easily handle conditionally censored data by incorporating time-varying censoring weights, and moreover, it allows for the inclusion of prior information via the sampling-importance resampling approach (Saarela et al., 2015). Bayesian methods are increasingly influential in applied causal inference, offering the ability to make direct probabilistic statements about treatment effects and to assess sensitivity with respect to alternative priors or expert-driven inputs. Despite these advantages, Bayesian causal methods for longitudinal data remain underdeveloped Liu et al. (2020). In this paper, we proposed a scalable Bayesian approach that effectively handles longitudinal data and is easily implementable. Our proposed Bayesian dose-response estimation is derived under the SUTVA assumption, assuming no interference. In our motivating COVID study, this assumption translates to each unit’s monthly metro-ridership exposure being assumed to affect only its own subsequent COVID-19 risk, which can be violated in application. Methodological extensions that relax SUTVA are emerging (O’Riordan and Gilligan-Lee, 2025). Future work will adapt these ideas to longitudinal, continuous-dose settings, enabling joint estimation of direct and indirect (spillover) ridership effects on COVID-19 dynamics. Despite this limitation, the proposed estimator fills an important methodological gap by coupling flexible non-parametric Bayesian inference with repeated-measures data and a time-varying continuous exposure. It remains fully appropriate for applications where interference is unlikely (e.g., individual risk-factor studies in chronic-disease epidemiology). Furthermore, our framework offers a robust foundation that broader spillover-aware extensions can build upon.

Acknowledgements

Yu Luo was supported by the Engineering & Physical Sciences Research Council (EPSRC) Grant EP/Y029755/1. Kuan Liu was supported by the Canadian Institutes of Health Research (CIHR) Grant AD7200183.

Code Accessibility

The code for the simulation studies is publicly available at https://github.com/yumcgill/Bayes_DoseResponse.

References

- Badr, H. S., H. Du, M. Marshall, E. Dong, M. M. Squire, and L. M. Gardner (2020). Association between mobility patterns and COVID-19 transmission in the USA: a mathematical modelling study. *The Lancet Infectious Diseases* 11, 1247–1254.
- Chamberlain, G. and G. W. Imbens (2003). Nonparametric applications of Bayesian inference. *Journal of Business & Economic Statistics* 21(1), 12–18.
- Chernozhukov, V., H. Kasahara, and P. Schrimpf (2021). Causal impact of masks, policies, behavior on early covid-19 pandemic in the U.S. *Journal of Econometrics* 220, 23—62.

- Cho, J.-H., D.-K. Kim, and E.-J. Kim (2022). Multi-scale causality analysis between covid-19 cases and mobility level using ensemble empirical mode decomposition and causal decomposition. *Physica A: Statistical Mechanics and its Applications* 600, 127488.
- Derqui, N., A. Koycheva, J. Zhou, T. D. Pillay, M. A. Crone, S. Hakki, J. Fenn, R. Kundu, R. Varro, E. Conibear, K. J. Madon, J. L. Barnett, H. Houston, A. Singanayagam, J. S. Narean, M. R. Tolosa-Wright, L. Moss crop, C. Rosadas, P. Watber, C. Anderson, E. Parker, P. S. Freemont, N. M. Ferguson, M. Zambon, M. O. McClure, R. Tedder, W. S. Barclay, J. Dunning, G. P. Taylor, and Ajit Lalvani on behalf of the INSTINCT and AT-ACCC study group (2023). Risk factors and vectors for SARS-CoV-2 household transmission: a prospective, longitudinal cohort study. *Lancet Microbe* 4, e397–408.
- Galvao, A. F. and L. Wang (2015). Uniformly semiparametric efficient estimation of treatment effects with a continuous treatment. *Journal of the American Statistical Association* 110(512), 1528–1542.
- Google LLC (2022). Google COVID-19 Community Mobility Reports.
- Graham, D. J., E. J. McCoy, and D. A. Stephens (2014). Quantifying causal effects of road network capacity expansions on traffic volume and density via a mixed model propensity score estimator. *Journal of the American Statistical Association* 109(508), 1440–1449.
- Hale, T., N. Angrist, R. Goldszmidt, B. Kira, A. Petherick, T. Phillips, S. Webster, E. Cameron-Blake, L. Hallas, S. Majumdar, and H. Tatlow (2021). A global panel database of pandemic policies (Oxford COVID-19 Government Response Tracker). *Nature Human Behaviour* 5, 529–538.
- Hill, J. L. (2011). Bayesian nonparametric modeling for causal inference. *Journal of Computational and Graphical Statistics* 20(1), 217–240.
- Hirano, K. and G. W. Imbens (2004). The propensity score with continuous treatments,. In A. Gelman and X.-L. Meng (Eds.), *Applied Bayesian modeling and causal inference from incomplete-data perspectives*, pp. 110–127. John Wiley & Sons.
- Islam, N., S. J. Sharp, G. Chowell, S. Shabnam, I. Kawachi, B. Lacey, J. M. Massaro, R. B. D’Agostino Sr, and M. White (2020). Physical distancing interventions and incidence of coronavirus disease 2019: natural experiment in 149 countries. *British Medical Journal* 370(m2743), 1–10.
- Jia, J. S., X. Lu, Y. Yuan, G. Xu, J. Jia, and N. A. Christakis (2020). Population flow drives spatio-temporal distribution of COVID- 19 in China. *Nature* 582, 389–394.
- Kennedy, E. H., Z. Ma, M. D. McHugh, and D. S. Small (2017). Non-parametric methods for doubly robust estimation of continuous treatment effects. *Journal of the Royal Statistical Society Series B: Statistical Methodology* 79(4), 1229–1245.
- Kissler, S. M., N. Kishore, M. Prabhu, D. Goffman, Y. Beilin, R. Landau, C. Gyamfi-Bannerman, B. T. Bateman, J. Snyder, A. S. Razavi, J. Gal, A. Bianco, J. Stone, D. Larremore, C. O. Buckee, D. Katz, and Y. H. Grad

- (2020). Reductions in commuting mobility correlate with geographic differences in SARS-CoV-2 prevalence in New York City. *Nature Communications* 11, 4674.
- Kraemer, M. U. G., C. Yang, B. Gutierrez, C. Wu, B. Klein, D. M. Pigott, L. Open COVID-19 Data Working Group, du Plessis, N. R. Faria, R. Li, W. P. Hanage, J. S. Brownstein, M. Layan, A. Vespignani, H. Tian, C. Dye, O. G. Pybus, and S. V. Scarpino (2020). The effect of human mobility and control measures on the COVID-19 epidemic in China. *Science* 368, 493–497.
- Li, F., P. Ding, and F. Mealli (2023). Bayesian causal inference: a critical review. *Philosophical Transactions of the Royal Society A* 381(2247), 20220153.
- Li, Y., X. Wang, H. Campbell, H. Nair, and for the Usher Network for COVID-19 Evidence Reviews (UNCOVER) group (2021). The association of community mobility with the time-varying reproduction number (R) of SARS-CoV-2: a modelling study across 330 local UK authorities. *Lancet Digit Health* 3(10), e676–e683.
- Liu, K., O. Saarela, B. M. Feldman, and E. Pullenayegum (2020). Estimation of causal effects with repeatedly measured outcomes in a Bayesian framework. *Statistical Methods in Medical Research* 29(9), 2507–2519.
- Luo, Y., D. A. Stephens, D. J. Graham, and E. J. McCoy (2023). Assessing the validity of Bayesian inference using loss functions. *arXiv preprint:2103.04086*.
- Manzira, C. K., A. Charly, and B. Caulfield (2022). Assessing the impact of mobility on the incidence of COVID-19 in Dublin City. *Sustainable Cities and Society* 80, 103770.
- Mathieu, E., H. Ritchie, E. Ortiz-Ospina, M. Roser, J. Hasell, C. Appel, C. Giattino, and L. Rodés-Guirao (2021). A global database of COVID-19 vaccinations. *Nature Human Behaviour* 5, 947–953.
- McGrail, D. J., J. Dai, K. M. McAndrews, and R. Kalluri (2020). Enacting social distancing policies corresponds with dramatic reduction in COVID19 infection rates. *PLoS ONE* 15(7), 1–9.
- Naimi, A. I., E. E. Moodie, N. Auger, and J. S. Kaufman (2014). Constructing inverse probability weights for continuous exposures: a comparison of methods. *Epidemiology* 25(2), 292–299.
- Newton, M. A. and A. E. Raftery (1994). Approximate Bayesian inference with the weighted likelihood bootstrap. *Journal of the Royal Statistical Society: Series B (Statistical Methodology)* 56(1), 3–26.
- Nugent, J. R. and L. B. Balzer (2023). A demonstration of modified treatment policies to evaluate shifts in mobility and covid-19 case rates in us counties. *American Journal of Epidemiology* 192(5), 762—771.
- O’Riordan, M. and C. M. Gilligan-Lee (2025). Local interference: Removing interference bias in semi-parametric causal models. *arXiv preprint arXiv:2503.18756*.
- Robins, J. M., M. A. Hernan, and B. Brumback (2000). Marginal structural models and causal inference in epidemiology. *Epidemiology* 11(5), 550–560.

- Romero García, C., Á. Briz-Redón, A. Iftimi, M. Lozano, J. De Andrés, G. Landoni, and M. Zanin (2023). Understanding small-scale covid-19 transmission dynamics with the granger causality test. *Archives of Environmental & Occupational Health* 78(5), 273–281.
- Rubin, D. B. (1981). The Bayesian bootstrap. *The Annals of Statistics* 9(1), 130–134.
- Saarela, O., D. A. Stephens, E. E. Moodie, and M. B. Klein (2015). On Bayesian estimation of marginal structural models. *Biometrics* 71(2), 279–288.
- Sethuraman, J. (1994). A constructive definition of Dirichlet priors. *Statistica Sinica* 4(2), 639–650.
- Steiger, E., T. Mussnug, and L. E. Kroll (2021). Causal graph analysis of COVID-19 observational data in German districts reveals effects of determining factors on reported case numbers. *PLoS ONE* 16(5), e0237277.
- Stephens, D. A., W. S. Nobre, E. E. M. Moodie, and A. M. Schmidt (2023). Causal inference under misspecification: adjustment based on the propensity score (with discussion). *Bayesian Analysis* 18(2), 639–694.
- Tchetgen, E. J. T., M. M. Glymour, J. Weuve, and J. Robins (2012). Specifying the correlation structure in inverse-probability-weighting estimation for repeated measures. *Epidemiology* 23(4), 644–646.
- Thomas, M. M., N. Mohammadi, and J. E. Taylor (2022). Investigating the association between mass transit adoption and covid-19 infections in us metropolitan areas. *Science of the total environment* 811, 152284.
- Vansteelandt, S. and A. Sjolander (2016). Revisiting g-estimation of the effect of a time-varying exposure subject to time-varying confounding. *Epidemiologic Methods* 5(1), 37–56.
- Xiong, C., S. Hu, M. Yang, W. Luo, and L. Zhang (2020). Mobile device data reveal the dynamics in a positive relationship between human mobility and COVID-19 infections. *Proceedings of the National Academy of Sciences* 117(44), 27087–27089.

Table 1: Simulation results for the dose-response function at three given doses: average estimate, average estimated variance, coverage (%). Summary of 1000 simulation runs.

Example 1				
Method		dose = 3	dose = 4	dose = 5
		(6.046)	(7.046)	(8.046)
COV-BB	Av Est	6.016	7.046	8.076
	Av Est Var	0.004	0.003	0.004
	Coverage	91.8	95.6	93.1
WOR-BB	Av Est	6.020	7.034	8.052
	Av Est Var	0.032	0.023	0.041
	Coverage	84.7	84.6	86.6
COV-DP	Av Est	6.020	7.049	8.079
	Av Est Var	0.004	0.003	0.004
	Coverage	97.7	98.5	98.3
WOR-DP	Av Est	6.011	7.050	8.089
	Av Est Var	0.021	0.013	0.022
	Coverage	97.8	98.4	97.9
Example 2				
Method		dose = 3	dose = 4	dose = 5
		(5.474)	(6.686)	(8.167)
COV	Av Est	5.294	6.633	8.285
	Av Est Var	0.017	0.018	0.031
	Coverage	72.7	93.4	88.5
WOR	Av Est	5.417	6.692	8.251
	Av Est Var	0.172	0.140	0.201
	Coverage	83.8	85.3	82.9
COV-DP	Av Est	5.301	6.639	8.293
	Av Est Var	0.017	0.018	0.029
	Coverage	91.8	95.6	93.1
WOR-DP	Av Est	5.459	6.723	8.271
	Av Est Var	0.110	0.140	0.138
	Coverage	94.8	98.8	97.5

Table 2: Descriptive statistics of metro ridership data

Variable	Description	Min.	Max.	Mean	Std. Dev.
Ridership (<i>log</i> scale)	Number of passengers per day in log scale	10.17	15.15	13.02	1.07
Cases ($\log(x + 1)$ scale)	Number of confirmed COVID-19 cases in $\log(x + 1)$ scale	4.52	14.31	10.24	1.81
Deaths	Number of confirmed COVID-19 deaths	12	121201	40167	37874.10
Stringency index	Stringency index ranging from 0-100 from OxCGRT. Represents degree of severity of policy measures to contain COVID-19 transmission.	20.37	98.46	62.44	16.04
Total vaccinations per hundred	Number of total vaccinations i.e. sum of all doses per hundred people of population. For vaccines that require multiple doses, each individual dose is counted.	0	238	56.40	71.87
Retail and recreation	Google mobility data for mobility changes relative to a baseline regular (pre-Covid) day for retail and recreation places	-97	36	-37	22.33
Grocery and pharmacy	Google mobility data for mobility changes relative to a baseline regular (pre-Covid) day for grocery and pharmacy places	-91	99	-9	20.16
Parks	Google mobility data for mobility changes relative to a baseline regular (pre-Covid) day for parks	-98	294	-3	51.67
Transit stations	Google mobility data for mobility changes relative to a baseline regular (pre-Covid) day for transit stations	-93	61	-41	21.80
Workplaces	Google mobility data for mobility changes relative to a baseline regular (pre-Covid) day for workplaces	-92	31	-35	21.77
Residential	Google mobility data for mobility changes relative to a baseline regular (pre-Covid) day for residential places	-9	48	13	8.75

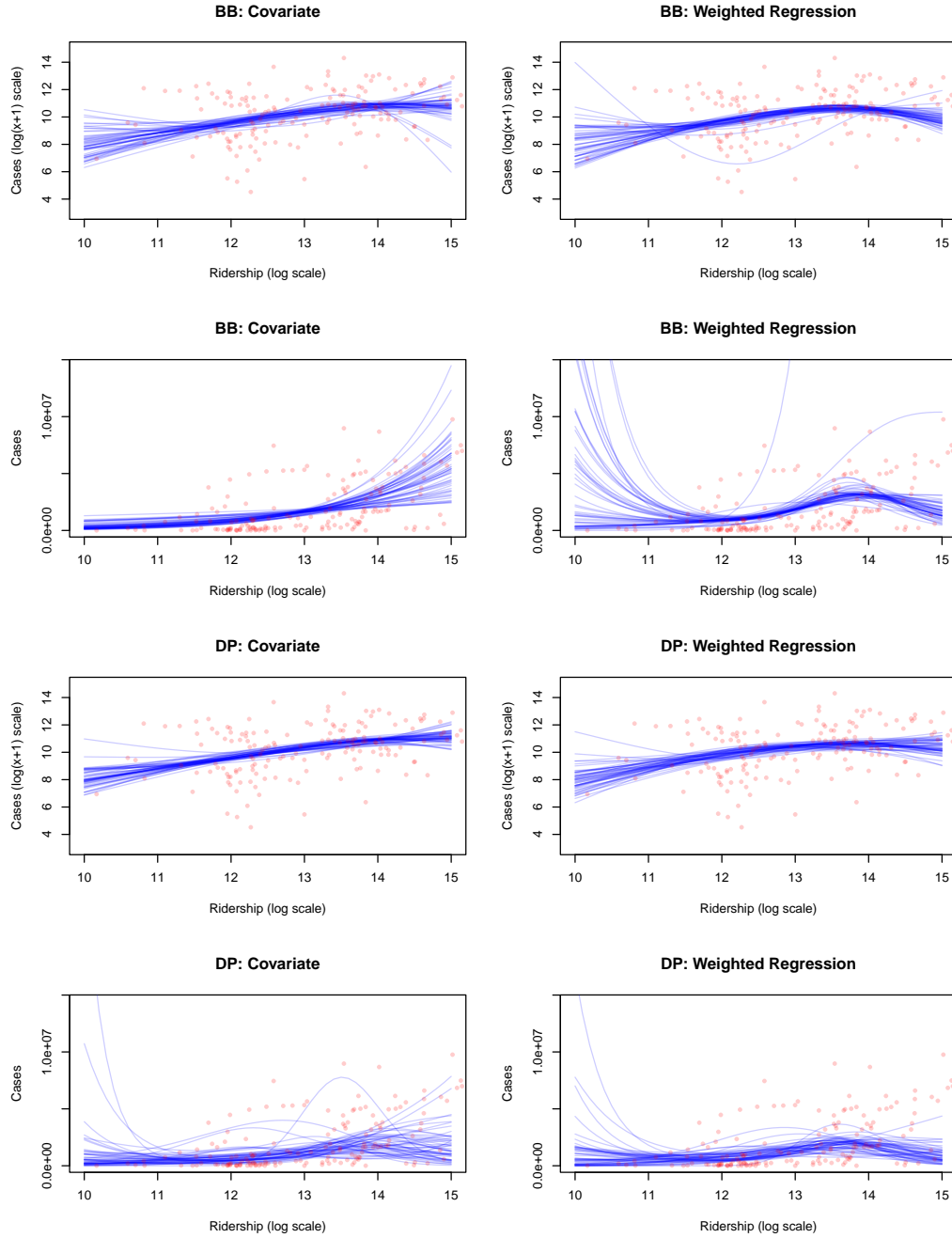


Figure 4: Application: Posterior dose-response curves using WOR (right panel) and COV (left panel) approaches WOR and COV approaches, with outcomes defined as $\log(\text{case} + 1)$ and cases.

Table 3: Posterior estimates of the dose-response function and associated APOs with credible intervals.

Outcome: $\log(\text{case} + 1)$				
Method		dose = 11	dose = 13	dose = 15
COV-BB	Posterior median	8.83	10.32	10.86
	Credible interval	(7.98, 9.76)	(9.72, 10.76)	(9.39, 12.40)
WOR-BB	Posterior median	8.85	10.35	9.95
	Credible interval	(8.00, 9.95)	(9.49, 10.71)	(8.86, 11.63)
COV-DP	Posterior median	8.90	10.30	11.11
	Credible interval	(8.30, 9.56)	(9.91, 10.30)	(10.06, 12.15)
WOR-DP	Posterior median	8.98	10.39	10.31
	Credible interval	(8.28, 9.72)	(9.93, 10.76)	(8.92, 11.81)
Outcome: Cases				
COV-BB	Posterior median	5.90×10^5	1.63×10^6	5.41×10^6
	Credible interval	$(2.07 \times 10^5, 1.2 \times 10^6)$	$(1.29 \times 10^6, 1.90 \times 10^6)$	$(2.22 \times 10^6, 1.13 \times 10^7)$
WOR-BB	Posterior median	1.19×10^6	1.90×10^6	1.52×10^6
	Credible interval	$(2.51 \times 10^5, 4.03 \times 10^6)$	$(1.46 \times 10^6, 3.24 \times 10^6)$	$(4.49 \times 10^5, 2.38 \times 10^7)$
COV-DP	Posterior median	4.17×10^5	1.05×10^6	1.69×10^6
	Credible interval	$(0.41 \times 10^5, 2.26 \times 10^6)$	$(3.85 \times 10^5, 3.34 \times 10^6)$	$(1.00 \times 10^5, 1.85 \times 10^7)$
WOR-DP	Posterior median	4.94×10^5	1.25×10^6	9.41×10^5
	Credible interval	$(0.69 \times 10^5, 1.66 \times 10^6)$	$(5.68 \times 10^5, 2.71 \times 10^6)$	$(0.90 \times 10^5, 7.10 \times 10^6)$